

# Development of a Selective Small-Molecule Inhibitor of Kir1.1, the Renal Outer Medullary Potassium Channel<sup>S</sup>

Gautam Bhawe, Brian A. Chauder, Wen Liu, Eric S. Dawson, Rishin Kadakia, Thuy T. Nguyen, L. Michelle Lewis, Jens Meiler, C. David Weaver, Lisa M. Satlin, Craig W. Lindsley, and Jerod S. Denton

Departments of Anesthesiology (G.B., R.K., T.T.N., J.S.D.) and Pharmacology (T.T.N., J.M., C.D.W., J.S.D.), Division of Nephrology (G.B.), Institute of Chemical Biology (B.A.C., E.S.D., L.M.L., C.W.L., J.S.D.), Digestive Disease Research Center (J.S.D.), Vanderbilt University School of Medicine, Nashville, Tennessee; and Division of Pediatric Nephrology, Department of Pediatrics, Mount Sinai School of Medicine, New York, New York (W.L., L.M.S.)

Received June 14, 2010; accepted October 6, 2010

## ABSTRACT

The renal outer medullary potassium ( $K^+$ ) channel, ROMK (Kir1.1), is a putative drug target for a novel class of loop diuretic that would lower blood volume and pressure without causing hypokalemia. However, the lack of selective ROMK inhibitors has hindered efforts to assess its therapeutic potential. In a high-throughput screen for small-molecule modulators of ROMK, we previously identified a potent and moderately selective ROMK antagonist, 7,13-bis(4-nitrobenzyl)-1,4,10-trioxa-7,13-diazacyclopentadecane (VU590), that also inhibits

Kir7.1. Because ROMK and Kir7.1 are coexpressed in the nephron, VU590 is not a good probe of ROMK function in the kidney. Here we describe the development of the structurally related inhibitor 2,2'-oxybis(methylene)bis(5-nitro-1*H*-benzo[*d*]imidazole) (VU591), which is as potent as VU590 but is selective for ROMK over Kir7.1 and more than 65 other potential off-targets. VU591 seems to block the intracellular pore of the channel. The development of VU591 may enable studies to explore the viability of ROMK as a diuretic target.

## Introduction

ROMK (Kir1.1) channels are expressed in the thick ascending limb (TAL) of Henle's loop, connecting tubule, and collecting duct (CD) segments of the nephron, where they mediate  $K^+$  secretion into the urinary filtrate (for review, see Hebert et al., 2005; Welling and Ho, 2009). In the TAL,

ROMK provides substrate  $K^+$  ions necessary for  $NaCl$  reabsorption by the  $Na^+-K^+-2Cl^-$  cotransporter and loop diuretic target. In the connecting tubule and CD, ROMK constitutes a key pathway for  $K^+$  secretion. A growing body of genetic (Ji et al., 2008; Tobin et al., 2008) and pharmacologic (Clark et al., 1993; Wang et al., 1995a; Wang et al., 1995b) evidence suggests that ROMK antagonists could act as potent diuretics by inhibiting  $Na^+$  reabsorption in the TAL and minimizing urinary  $K^+$  loss through their actions in the CD. Thus, ROMK-directed diuretics hold the potential to avoid hypokalemia, a serious side effect of conventional loop and thiazide diuretics used in the treatment of hypertension and congestive heart failure (Grobbee and Hoes, 1995; Macdonald and Struthers, 2004).

The idea that ROMK antagonists will induce diuresis with minimal  $K^+$  wasting is not new. In the 1990s, Wang et al. (1995a,b) and Clark et al. (1993) characterized the renal consequences of two  $K_{ATP}$  blockers exhibiting comparatively weak off-target activity toward apical TAL and CD small-conductance  $K^+$  channels, which are now known to be medi-

This work was supported by the National Institutes of Health National Institute of Neurological Disorders and Stroke [Grant 1R21-NS57041-1]; the National Institutes of Health National Institute of Diabetes and Digestive and Kidney Diseases [Grants 1R01-DK082884, DK038470, P30-DK079307]; the National Institutes of Health National Institute of General Medical Sciences [Grants R01-GM080403, T32-GM07628]; the National Institutes of Health National Institute of Mental Health [Grants U54MH074427, 1U54-MH084659]; the American Heart Association Southeast Affiliate [Beginning Grant-in-Aid 0865106E]; and the National Kidney Foundation [Postdoctoral Fellowship].

G.B. and B.A.C. contributed equally to this work.

Article, publication date, and citation information can be found at <http://molpharm.aspetjournals.org>.  
doi:10.1124/mol.110.066928.

<sup>S</sup> The online version of this article (available at <http://molpharm.aspetjournals.org>) contains supplemental material.

**ABBREVIATIONS:** ROMK, renal outer medullary potassium ( $K^+$ ) channel; TAL, thick ascending limb; hERG, human *ether-à-go-go*-related gene; HEK, human embryonic kidney; cRNA, 7-methyl guanosine-capped RNA; BNBI, 1,3-bis(5-nitro-1*H*-benzo[*d*]imidazol-2-yl)propane; DMSO, dimethyl sulfoxide; CD, collecting duct; Kir, inward rectifying potassium; BK, large conductance  $K^+$  channels; TPNQ, tertiapin-Q; ABS, antenatal Bartter syndrome; VU590, 7,13-bis(4-nitrobenzyl)-1,4,10-trioxa-7,13-diazacyclopentadecane; VU591, 2,2'-oxybis(methylene)bis(5-nitro-1*H*-benzo[*d*]imidazole).

ated at least in part by ROMK. At high doses, these compounds induced natriuresis and diuresis but had very little effect on urinary  $K^+$  excretion. Although these studies provided a glimpse into the therapeutic potential of ROMK, the agents were limited by low potency toward ROMK and undesirable cardiovascular and metabolic side effects mediated by  $K_{ATP}$  channels.

We recently performed a high-throughput screening of approximately 125,000 small molecules for chemical modulators of ROMK (Lewis et al., 2009). Several antagonists were discovered, including a submicromolar ROMK inhibitor, 7,13-bis(4-nitrobenzyl)-1,4,10-trioxo-7,13-diazacyclopentadecane (VU590), that also weakly inhibits Kir7.1. Because ROMK and Kir7.1 are coexpressed in the nephron, VU590 cannot be used as a selective ROMK probe in the kidney. Here we describe the development of a novel inhibitor termed VU591 that is equally potent and highly selective for ROMK.

## Materials and Methods

### Expression Vectors

Plasmids used in this study are from the following sources: rat ROMK1 (NM\_017023; Chun Jiang, Georgia State University, Atlanta, GA), human Kir2.1 (NM\_000891.2; Al George, Vanderbilt University School of Medicine, Nashville, TN), human Kir7.1 (NM\_002242.2; David Clapham, Harvard Medical School, Cambridge, MA), human Slo1/KCNMA1 (NM\_001014797; Jianmin Cui, Washington University, St. Louis, MO), human KCNMB1 (NM\_004137; Robert Brenner, University of Texas Health Science Center at San Antonio, San Antonio, TX), and human *ether-à-go-go*-related gene (hERG; Sabina Kupersmidt, Vanderbilt University School of Medicine); mouse Kir6.2 (NM\_010602) and hamster SUR1 (L40623.1) vectors are from Colin Nichols (Washington University). Human ROMK1 (NM\_000220), Kir2.3 (NM\_152868), Kir4.1 (NM\_002241), and Kv1.3 (NM\_002232.2) were purchased from OriGene Technologies (Rockville, MD).

### Cell Lines and Transfections

Thallium ( $Tl^+$ )-flux assays and parallel patch clamp experiments (see *Automated Patch-Clamp Electrophysiology*) were performed using the C1 monoclonal tetracycline-regulatable HEK-293 cell line expressing ROMK1-S44D described previously (Lewis et al., 2009). For conventional patch-clamp experiments, HEK-293 cells (American Type Culture Collection; Manassas, VA) were transiently co-transfected with channel expression vector and pcDNA3.1-EGFP (transfection marker) using Lipofectamine 2000 (Invitrogen, Carlsbad, CA) as described previously (Fallen et al., 2009) or FuGENE 6 (Roche Applied Science, Indianapolis, IN) according to the manufacturer's instructions.

### Thallium Flux Assays

$Tl^+$  flux assays were performed as described in detail previously (Lewis et al., 2009). In brief, C1 cells cultured overnight in a 384-well plate containing serum-free media and tetracycline were loaded with the  $Tl^+$ -sensitive fluorescent dye FluxOR (Invitrogen). Assays were performed on a Hamamatsu Functional Drug Screening System 6000. Cells were incubated for 20 min with small molecules before  $Tl^+$  addition. The normalized rate of flux between 7 and 12 s after  $Tl^+$  addition is reported.

### Conventional Patch-Clamp Electrophysiology

Conventional patch clamp experiments were performed essentially as described previously (Fallen et al., 2009). The standard intracellular solution contained 135 mM KCl, 2 mM  $MgCl_2$ , 1 mM EGTA, 10 mM HEPES-K, and 2 mM  $Na_2ATP$  (Roche), pH 7.3, adjusted to 275 mOsmol/kg with sucrose. For Kir2.3 recordings,  $MgCl_2$

was reduced to 1 mM to prevent channel rundown (Chuang et al., 1997). Kir6.2 recordings were made with 0.5 mM  $MgCl_2$  in the absence of ATP to eliminate ATP-induced channel inhibition. Slo1/ $\beta$ 1 recordings were conducted with 1 mM EGTA and 0.1 mM  $CaCl_2$  without ATP or  $MgCl_2$ . The standard bath solution contained 135 mM NaCl, 5 mM KCl, 2 mM  $CaCl_2$ , 1 mM  $MgCl_2$ , 5 mM glucose, and 10 mM HEPES- $Na^+$ , pH 7.4, 290 mOsmol/kg. In some experiments, a high- $K^+$  bath was used that contained 90 mM NaCl, 50 mM KCl, 2 mM  $CaCl_2$ , 1 mM  $MgCl_2$ , 5 mM glucose, and 10 mM HEPES- $Na^+$ , pH 7.4, 290 mOsmol/kg.

For Kir current recordings, cells were voltage-clamped and stepped every 5 s from a holding potential of  $-75$  to  $-120$  mV for 200 ms, then ramped at a rate of 2.4 mV/ms to 120 mV before returning to  $-75$  mV (Fig. 2C, inset). Kv1.3 currents were evoked using a similar protocol, except  $V_m$  was ramped from  $-120$  to 0 mV every 10 s. Slo1/ $\beta$ 1 currents were recorded every 5 s after 200-ms voltage step to 100 mV from a holding potential of  $-75$  mV.

After achieving stable whole-cell currents, VU591 was applied intermittently or continuously for 4 to 10 min. This was followed by application of a known channel blocker (i.e., 2 mM barium, Kir channels; 2 mM tetraethylammonium, Slo1/ $\beta$ 1 channels; 1 mM 4-aminopyridine, Kv1.3; or dofetilide, hERG) as a positive control.

### Automated Patch-Clamp Electrophysiology

Parallel patch-clamp experiments were performed using a Patchliner workstation (Nanion Technologies; Munich, Germany) that enables fully automated patch-clamp recordings to be made from up to eight cells simultaneously (Milligan et al., 2009). The Patchliner uses disposable NPC-16 microfluidic recording chambers containing an array of 16 individual planar glass electrodes with apertures of defined geometry and resistance. Medium-resistance (1.8–3.0 M $\Omega$ ) chambers were used in the present study. Eight channels can be recorded from concurrently using two EPC-10 Quadro amplifiers (HEKA, Lambrecht/Pfalz, Germany). A programmable robotic probe is used for solution exchanges. A typical experiment was performed as follows. The lower (35- $\mu$ l volume) and upper (15- $\mu$ l volume) chambers were filled with intracellular and extracellular recording solutions, respectively. The intracellular solution contained 50 mM KCl, 10 mM NaCl, 60 mM KFI, 2 mM  $MgCl_2$ , 10 mM EGTA, and 20 mM HEPES, pH 7.2, 275 mOsmol/kg. The standard extracellular solution was identical to that used for conventional patch-clamp experiments described above. Overnight tetracycline-induced C1 cells (Lewis

et al., 2009) were dissociated by brief trypsinization, diluted to a concentration of  $10^6$  cells/ml and added to the upper chamber of the recording chamber where one cell is pulled by gentle suction into the aperture separating the two compartments. A series of automated vacuum steps is delivered to the internal chamber to establish a gigaohm seal and whole-cell access. A "seal enhancer" solution containing 80 mM NaCl, 3 mM KCl, 10 mM  $MgCl_2$ , 35 mM  $CaCl_2$ , and 10 mM HEPES, pH 7.4, is added to the external compartment to facilitate seal formation. After establishing the whole-cell configuration, seal enhancer was exchanged for standard bath solution and the voltage-clamp experiment was initiated. Cells were voltage-clamped from a  $-75$  mV holding potential and stepped for 200 ms every 10 s to a test pulse of  $-120$  mV. For dose-response experiments, 45  $\mu$ l of test compounds of increasing concentration were added to the external compartment followed by a final addition of 2 mM  $Ba^{2+}$  to measure leak current. Cells exhibiting an unstable baseline or less than 90%  $Ba^{2+}$ -inhibitable current at  $-120$  mV were excluded from analysis.

### Preparation of *Xenopus laevis* Oocytes

Stage V–VI oocytes from the African clawed frog *X. laevis* were generously provided by Dr. Eric Delpire (Vanderbilt University School of Medicine, Nashville, TN). The oocyte follicle layer was removed by manual dissection after enzymatic treatment with 2

mg/ml collagenase (type 1A Sigma) dissolved in calcium-free OR-2 of the following composition 82.5 mM NaCl, 2 mM KCl, 1 mM MgCl<sub>2</sub>, and 5 mM HEPES, adjusted to pH 7.5 with NaOH. Oocytes were allowed to recover overnight at 16°C in L-15 media diluted 50% with 18 MΩ water and containing gentamicin sulfate (25 mg/ml).

### RNA Transcription and Injection

A plasmid encoding the hERG was linearized with EcoRI and used as a template to transcribe 7-methyl guanosine-capped RNA (cRNA) with the SP6 RNA polymerase and nucleotides provided in the mMESSAGE mMACHINE kit (Ambion, Austin, TX). cRNA was purified by LiCl precipitation, diluted in RNAase-free water and used for injections. Five to fifty nanograms of hERG cRNA in 50 nl of water was injected into each oocyte using a Drummond digital microdispenser. Oocytes were incubated at 16°C in modified L-15 for 24 to 48 h before hERG recordings.

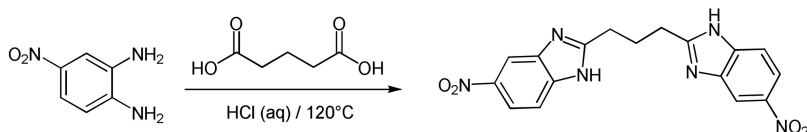
### Two-Electrode Voltage-Clamp Analysis

Whole-cell currents were recorded from *X. laevis* oocytes injected with hERG cRNA using the two-electrode voltage-clamp technique. Current and voltage commands were generated with a GeneClamp 600 amplifier, a Digidata 1200 A/D converter, and pClamp 8.0 software (Molecular Devices, Sunnyvale, CA). The bath was actively clamped to 0 mV using a VG-2A bath clamp (Molecular Devices). Electrodes pulled from borosilicate glass (Sutter Instruments, Novato, CA) using a vertical puller (PP-830; Narishige International, Narishige, Japan) had resistances of 0.5 to 5.0 MΩ when filled with 3 M KCl. The standard bath solution contained 85 mM NaCl, 5 mM KCl, 10 mM HEPES, and 2 mM MgCl<sub>2</sub>, pH adjusted to 7.4 with NaOH. VU591 and the hERG channel inhibitor dofetilide (positive control; Tocris Biosciences) were tested at 10 μM.

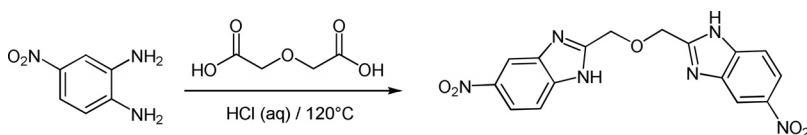
hERG currents were evoked as follows. From a holding potential of -80 mV, the oocyte potential was stepped to -20 mV for 2 s and returned to -80 mV to elicit inward hERG tail currents. This protocol was repeated every 20 to 30 s. hERG currents were pharmacologically isolated from endogenous oocytes currents by subtracting the tail current at -80 mV from the time-independent current remaining after maximal hERG blockade with 10 μM dofetilide (Supplemental Fig. 5).

### Chemical Synthesis

**1,3-Bis(5-nitro-1H-benzo[d]imidazol-2-yl)propane.** A suspension of 4-nitrobenzene-1,2-diamine (300 mg, 1.96 mmol) and glutaric acid (130 mg, 0.98 mmol) in 5 N HCl (2 ml) was heated to 120°C (bath temp) in a sealed tube. A solution forms in 1 h. After 12 h of heating, the mixture was cooled to room temperature and poured into saturated NaHCO<sub>3</sub> solution (50 ml) and the pH was adjusted to 8. The mixture was filtered and the product was washed with water. The product was dried in a vacuum oven for 10 h to afford BNBI as a light brown solid (260 mg, 72%). The product was recrystallized from absolute EtOH to give BNBI as a colorless solid. <sup>1</sup>H-NMR (400 MHz, DMSO-*d*<sub>6</sub>) δ 8.37(d, *J* = 2.1 Hz, 2H), 8.11 (dd, *J* = 8.8, 2.1 Hz, 2H), 7.69 (d, *J* = 8.8 Hz, 2H), 3.10 (t, *J* = 7.3 Hz, 4H), 2.42 (q, *J* = 7.3 Hz, 2H); liquid chromatography/mass spectrometry (*m/z*) = 367 (M + H) (Scheme 1).



Scheme 1. BNBI.



Scheme 2. VU591.

**VU591.** A suspension of 4-nitrobenzene-1,2-diamine (300 mg, 1.96 mmol) and diglycolic acid (131 mg, 0.98 mmol) in 5 N HCl (2 ml) was heated to 120°C (bath temperature) in a sealed tube. A solution forms in 1 h. After 12 h of heating, the mixture was cooled to room temperature and poured into saturated NaHCO<sub>3</sub> solution (50 ml) and the pH was adjusted to 8. The mixture was filtered and the product was washed with water. The product was dried in a vacuum oven for 10 h to afford VU591 as a light brown solid (368 mg, 51%). The product was recrystallized from absolute EtOH to give VU591 as a colorless solid. <sup>1</sup>H-NMR (400 MHz, DMSO-*d*<sub>6</sub>) δ 8.46 (d, *J* = 1.3 Hz, 2H), 8.11 (dd, *J* = 8.8, 1.3 Hz, 2H), 7.73 (d, *J* = 8.8 Hz, 2H), 5.00 (s, 4H); HRMS (calculated for C<sub>16</sub>H<sub>12</sub>N<sub>6</sub>O<sub>5</sub>+H) 369.0947; Found 369.0947 (Scheme 2).

**VU590.** VU590 used in this study was synthesized locally as described previously (Lewis et al., 2009). However, VU590 is now commercially available from Sigma-Aldrich and Tocris Bioscience.

### Plasma Protein Binding

Human or rat plasma samples spiked with 10 mM VU591, warfarin (control), or verapamil (control) dissolved in DMSO were added in the cis chambers of rapid equilibrium dialysis plates (Thermo Fisher Scientific, Waltham, MA). Dulbecco's phosphate-buffered saline was added to the corresponding trans compartment. The samples were dialyzed for 4 h at 37°C with shaking, after which the proteins were extracted using ice-cold acetonitrile containing 0.1% formic acid and an internal standard at a concentration of 50 ng/ml. The extracts were analyzed by means of high-performance liquid chromatography/tandem mass spectrometry, using a ThermoFinnigan TSQ Quantum Ultra (Thermo Fisher Scientific, Waltham, MA) mass spectrometer operating in the positive ion mode, by selective reaction monitoring. Percentage of unbound VU591 was calculated based on the percentage of compound in the PBS chamber compared with that of the total in the PBS and plasma chambers.

### Metabolic Stability

VU591, verapamil (control), or propranolol (control) were incubated at 37°C for 15 min with constant shaking in solution containing rat or human liver microsomes, phosphate-buffered saline, and NADPH as a cofactor. After incubation, the samples were extracted using ice-cold acetonitrile containing 0.1% formic acid and an internal standard. The extracts were analyzed by means of high-performance liquid chromatography/tandem mass spectrometry. Percentage of test compound remaining after incubation was calculated based on the amount of compound in the incubated samples compared with identically prepared control samples not incubated with microsomes.

### Molecular Modeling

SurflexSim (SybylX 1.1; Tripos International, St. Louis, MO) was applied to generate 100 mutual flexible alignment hypotheses for the three-dimensional superposition of BNBI and VU591. The algorithm is based on morphological similarity, a method that attempts to gauge molecular similarity from the point of view of the protein target via a fragment-based flexible alignment of small molecules with known activity. In brief, this method makes use of a three-

dimensional grid of observer points in which minimum distances to the van der Waals surface, a hydrogen-bond acceptor or negatively charged atom, and a hydrogen-bond donor or positively charged atom are employed in conformational sampling with the addition of a restraining term to prevent excessive steric clash and a directionality term to capture observations of polar features (Jain, 2000). The best scoring alignment for BNBI/VU591 was taken as a template for the flexible alignment of VU590 using SurfexSim to explore the potential three-dimensional conformational similarity of these molecules. Visualization of surface electrostatic properties for VU590, BNBI, and VU591 was performed by mapping atom-centered partial charges from the Merck Molecular Mechanics Force Field (MMFF94) onto Connolly surfaces that were generated for the most similar conformers of each compound and rendered in PyMol (<http://www.pymol.org>).

## Statistics

Unless noted otherwise, results are expressed as means  $\pm$  S.E.M.;  $n$  equals the number of replicates. To calculate the half-inhibition concentration of VU591 for rat ROMK (Table 1), the unaveraged concentration-response data from between four and seven cells at each concentration were fit to a four parameter logistic equation in Excel 2007 (Microsoft) using the XLfit add-in (ID Business Solutions). The top and bottom parameters were constrained at 100% as defined by control traces run before test compound exposure for each cell and 0% as defined by currents measured in four cells with a fully effective concentration of barium. The voltage-dependence of VU591 block was assessed using univariate statistics with paired  $t$  test conducted using commercially available statistical software (SigmaStat; SPSS Inc., Chicago, IL). Multivariate statistics used a generalized linear model (GLM) accounting for repeated measures and were performed with  $R$ -software version 2.10.0 (<http://www.r-project.org>). In all analyses, a two-sided  $P$  value  $<0.05$  was required to reject the null hypothesis.

## Results

**BNBI Inhibits ROMK but Not Kir7.1.** VU590 is a bis-nitro-benzyl compound (Fig. 2A, top) that inhibits ROMK at submicromolar concentrations but has no effect on Kir2.1 or Kir4.1. VU590 is only moderately selective, however, because it also inhibits Kir7.1 at low micromolar concentrations (Lewis et al., 2009). Because ROMK and Kir7.1 are coexpressed in the nephron (Ookata et al., 2000), VU590 can not be used to selectively assess ROMK function in the kidney.

In an effort to identify a more selective inhibitor, we tested a structurally related hit from the primary screen, BNBI (Fig. 2A, middle), for activity toward ROMK and Kir7.1. BNBI was resynthesized and examined in whole-cell patch-

clamp experiments. Its effects on ROMK were tested in stably transfected C1 cells (see *Materials and Methods*) using a Patchliner parallel patch clamp workstation (Milligan et al., 2009). As shown in Fig. 1A, BNBI inhibited ROMK current at  $-120$  mV in a dose-dependent manner at 1, 5, and 10  $\mu\text{M}$ . The mean  $\pm$  S.E.M. concentration-response curves for BNBI, and VU590 for comparison, are shown in Fig. 1B. Compared with VU590, ROMK inhibition by BNBI was weak and incomplete. However, we found that unlike VU590, which inhibited Kir7.1 by  $58.3 \pm 2.4\%$  ( $n = 3$ ) at 10  $\mu\text{M}$ , BNBI at concentrations up to 100  $\mu\text{M}$  had no significant ( $P > 0.05$ ;  $n = 3$ ) effect on Kir7.1 activity (Fig. 1C). We therefore initiated medicinal chemistry efforts around the BNBI scaffold with the goal of improving its potency and maintaining its selectivity.

Figure 2A shows the chemical structures of VU590 (top) and BNBI (middle) with substructural regions of similar topology highlighted in bold. Each compound contains two nitro ( $\text{NO}_2$ ) groups flanking a variable seven-atom linker region harboring two nitrogen atoms. A key difference between VU590 and BNBI is the absence of a central oxygen atom within the linker of BNBI. Given the increased polarity and hydrogen bond acceptor potential of the VU590 linker, we hypothesized that the addition of an ether oxygen to the BNBI linker would increase potency toward ROMK by providing additional interactions between the channel and ether oxygen lone pair electrons (see *Discussion*). Indeed, the resulting compound, VU591 (Fig. 2A, bottom), was almost 30-fold more potent at inhibiting ROMK than was BNBI. In  $\text{Ti}^+$  flux assays, VU591 inhibited ROMK with an  $\text{IC}_{50}$  of 240 nM, whereas BNBI inhibited ROMK with a  $\text{IC}_{50}$  of approximately 8  $\mu\text{M}$  (Fig. 2B).

**VU591 Is a Selective ROMK Inhibitor.** We next examined the selectivity of VU591 across several inward rectifier and voltage-gated  $\text{K}^+$  channels expressed in HEK-293 cells. Cells were voltage ramped between  $-120$  mV and 120 mV every 5 s from a holding potential of  $-75$  mV (Fig. 2C, inset). ROMK-mediated inward current at  $-120$  mV was inhibited by 10  $\mu\text{M}$  VU591 with a monoexponential time course. Wash-out was very slow and incomplete, and the presence of VU591 did not prevent additional block by extracellular barium (Fig. 2C). As illustrated in Fig. 2D and quantified in Fig. 3C, VU591 block in a physiological  $\text{K}^+$  gradient (5 mM extracellular, 135 mM intracellular) was effective at both negative and positive potentials.

Consistent with the  $\text{Ti}^+$  flux data (Fig. 2B), VU591 inhib-

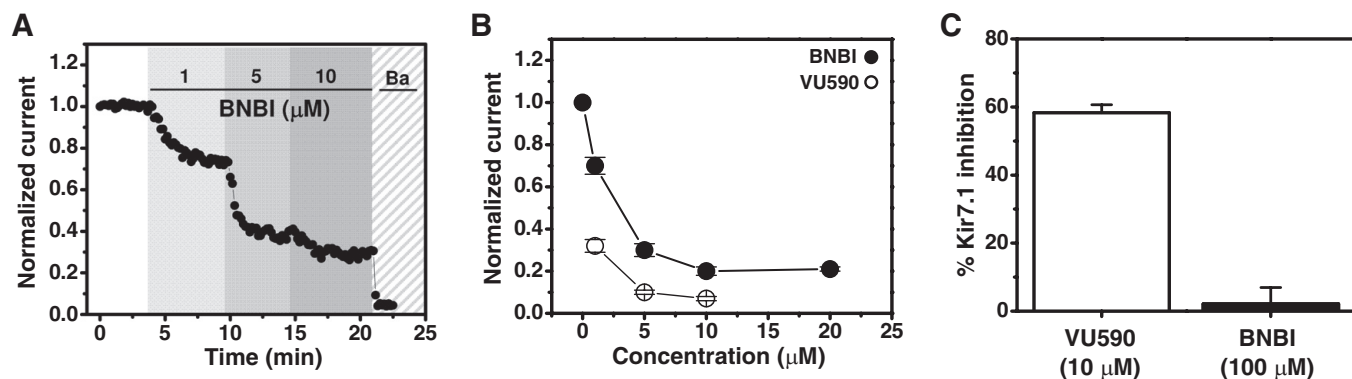


**Fig. 1.** BNBI inhibits ROMK but not Kir7.1. Representative whole-cell patch-clamp experiment showing dose-dependent inhibition of ROMK-S44D by BNBI. Normalized current ( $I_{\text{BNBI}}/I_{\text{Control}}$ ) recorded at  $-120$  mV is shown. Barium (Ba; 2 mM) was used to measure leak current at the end of every experiment. Data shown in A and B were acquired using a Patchliner automated patch-clamp workstation (see *Materials and Methods*). B, mean  $\pm$  S.E.M. concentration-response data for BNBI ( $n = 5$ ) and VU590 ( $n = 5$ ) are shown for comparison. C, mean  $\pm$  S.E.M. percentage inhibition by VU590 (10  $\mu\text{M}$ ) and BNBI (100  $\mu\text{M}$ ) of Kir7.1 current at  $-120$  mV in conventional patch-clamp experiments ( $n = 3-4$ ).

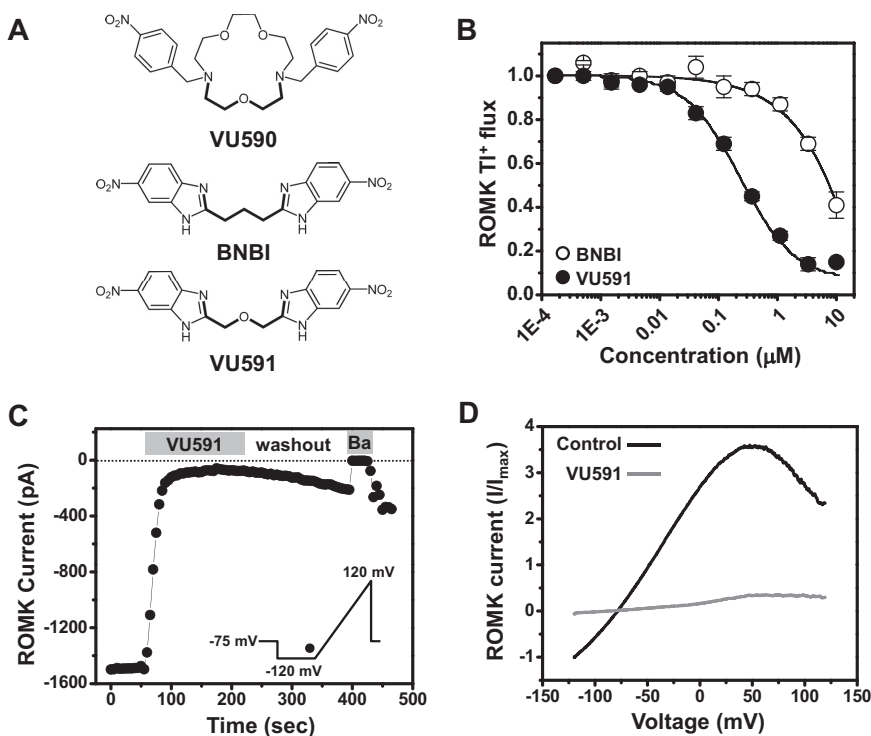
ited rat ROMK dose dependently with an  $IC_{50}$  of 300 nM (Table 1), which is virtually identical to that of VU590 ( $IC_{50}$ , 290 nM; Lewis et al., 2009). Thus, VU591 does not significantly improve upon the potency of VU590 toward ROMK. Block by VU591 reached a maximum of approximately 90% at 10  $\mu$ M, because block by 30  $\mu$ M VU591 was not significantly ( $P > 0.05$ ) different (Table 1). VU591 also blocked human ROMK. VU591 had no effect on Kir7.1 at 10  $\mu$ M, a concentration at which VU590 inhibited the channel by ~60% (Fig. 1C), and it did not inhibit Kir2.1, Kir2.3, and

TABLE 1

VU591 is a selective ROMK channel inhibitor

Mean  $\pm$  S.E.M. percentage inhibition by VU591 of the indicated  $K^+$  channel. Whole-cell currents were recorded from HEK-293 cells transfected with rat ( $n = 4-8$ ) or human ( $n = 4$ ) ROMK1, human Kir2.1 ( $n = 6$ ), human Kir2.3 ( $n = 5$ ), human Kir4.1 ( $n = 4$ ), mouse Kir6.2/hamster SUR1 ( $n = 3-8$ ), human Kir7.1 ( $n = 4$ ), Slo1/ $\beta$ 1 ( $n = 4$ ), or Kv1.3 ( $n = 4$ ). hERG currents ( $n = 6-8$ ) were recorded from *X. laevis* oocytes. Voltage-clamp protocols are described under *Materials and Methods*. Barium (2 mM), tetraethylammonium (2 mM), 4-aminopyridine (1 mM), and dofetilide (10  $\mu$ M) were used as control blockers of KirX, Slo1/ $\beta$ 1, Kv1.3, and hERG, respectively. Representative current traces for KirX, Slo1/ $\beta$ 1, Kv1.3, and hERG are shown in Supplemental Figs. S2 to S5, respectively.

Channel	Inhibition		
	VU591 $\mu$ M	VU591 %	Control Blocker
Rat ROMK	0.3	54 $\pm$ 4	94 $\pm$ 2
Rat ROMK	1	63 $\pm$ 2	
Rat ROMK	3	77 $\pm$ 4	
Rat ROMK	10	89 $\pm$ 1	
Rat ROMK	30	91 $\pm$ 2	
Human ROMK	10	86 $\pm$ 2	96 $\pm$ 1
Kir2.1	10	-4 $\pm$ 3	98 $\pm$ 1
Kir2.3	10	6 $\pm$ 6	91 $\pm$ 3
Kir4.1	10	-10 $\pm$ 4	96 $\pm$ 2
Kir6.2/SUR1B	10	17 $\pm$ 4	98 $\pm$ 1
Kir6.2/SUR1B	50	28 $\pm$ 3	
Kir7.1	10	5 $\pm$ 8	91 $\pm$ 2
Slo1/ $\beta$ 1	10	-4 $\pm$ 2	72 $\pm$ 3
Kv1.3	10	-5 $\pm$ 4	73 $\pm$ 6
hERG	10	25 $\pm$ 2	94 $\pm$ 1



**Fig. 2.** Development of a BNBI analog with improved potency toward ROMK. A, molecular structures of VU590, BNBI, and VU591. Atom connectivity is shown in bold to highlight regions of common topology. B, concentration-response curves for BNBI (○) and VU591 (●) mediated inhibition of  $TI^+$  flux through ROMK-S44D. Means  $\pm$  S.E.M. ( $n = 5$ ). C, representative time course of 10  $\mu$ M VU591-dependent ROMK inhibition, incomplete washout and block by 2 mM barium (Ba). Cells were voltage-ramped between -120 and 120 mV at a rate of 2.4 mV/ms every 5 s from a holding potential of -75 mV (inset). Currents at -120 mV are shown. D, ROMK current-voltage relationship recorded in the absence (control) or during steady-state block by 10  $\mu$ M VU591.

Kir4.1. At 10 and 50  $\mu$ M, respectively, VU591 inhibited Kir6.2/SUR1 currents by 17  $\pm$  4 and 28  $\pm$  3% (Table 1), which still affords a 150-fold selectivity window for ROMK over Kir6.2/SUR1. Representative steady-state current traces and time course data are shown in Supplemental Figs. 1 and 2, respectively.

We broadened our selectivity analysis to include two voltage-gated  $K^+$  (Kv) channels that are known to contribute to  $K^+$  secretion in the nephron: calcium- and voltage-activated large conductance  $K^+$  (BK) channels and Kv1.3. BK channels composed of channel-forming Slo1 (*KCNMA1*)  $\alpha$ - and regulatory  $\beta$ -subunits (*KCNMB*) have emerged recently as important regulators of distal nephron  $K^+$  secretion. Knockout studies in mice have shown that loss of Slo1 or  $\beta$ 1 expression reduces the kaliuretic response to high urinary flow rates (Pluznick et al., 2003; Grimm and Sansom, 2007; Rieg et al., 2007). Off-target activity toward BK channels could therefore erroneously assign a role for ROMK in the physiological response to VU591. We therefore tested whether VU591 inhibits heterologously expressed Slo1/ $\beta$ 1 BK channels. At a concentration of 10  $\mu$ M, VU591 had no significant ( $P > 0.05$ ;  $n = 5$ ) effect on Slo1/ $\beta$ 1 currents (Table 1). Representative BK current traces and a time course experiment are shown in Supplemental Fig. 3.

Kv1.3 was shown recently to contribute to  $K^+$  secretion in the CD of rats fed a high-K diet (Carrisoza-Gaytán et al., 2010). We therefore determined whether VU591 inhibits human Kv1.3 heterologously expressed in HEK-293 cells. As shown in Table 1, 10  $\mu$ M VU591 did not inhibit Kv1.3. Representative Kv1.3 current traces and a time-course experiment are shown in Supplemental Fig. 4. We reported previously (Lewis et al., 2009) that VU590 inhibits the mixed Kv current endogenously expressed in HEK-293 cells (Yu and Kerchner, 1998; Jiang et al., 2002). Messenger RNA for Kv1.3 is prominently expressed in HEK-293 cells and is therefore likely to contribute to the endogenous current

(Jiang et al., 2002). Consistent with the Kv1.3 heterologous expression data, VU591 had no significant ( $P > 0.05$ ;  $n = 4$ ) effect on the native HEK-293 current (mean  $\pm$  S.E.M. current at 60 mV in control and VU591-containing buffer were  $251 \pm 82$  and  $256 \pm 84$  pA, respectively).

Analysis of potential off-target activity was expanded further to include a panel of 68 critical targets, including several cardiac and central nervous system ion channels and receptors using the LeadProfilingScreen system from Ricerca Biosciences (Concord, OH). In this system, radioligand displacement assays are used to screen for small molecule activity against a target of interest, and values indicating percentage of ligand displacement are reported. VU591 had no effect on [ $^3$ H]astemizole binding of hERG channels, an off-target associated with lethal ventricular arrhythmias (Supplemental Table 1). However, we found in two-electrode voltage-clamp experiments on *X. laevis* oocytes that 10  $\mu$ M VU591 inhibited

hERG tail currents at  $-80$  mV (Supplemental Fig. 5) by approximately 25% (Table 1). Whether the discrepancies between radioligand binding and electrophysiological data reflect voltage- or use-dependent hERG channel block will be assessed in future studies.

Only four targets (GABA<sub>A</sub> receptor, dopamine D4 receptor, dopamine transporter, and norepinephrine transporter) exhibited greater than 50% radioligand displacement with 10  $\mu$ M VU591 (Supplemental Table 1), a threshold commonly used to prioritize hits from a high-throughput screening. These activities were further characterized with full CRCs in functional assays. Only the GABA<sub>A</sub> receptor exhibited an IC<sub>50</sub> below 10  $\mu$ M (IC<sub>50</sub> = 6.2  $\mu$ M), which still affords a 25-fold selectivity window for ROMK.

**VU591 Is a Pore Blocker.** Given the structural similarities between VU590 and VU591 (Fig. 2A), we hypothesize that they share a common binding site in ROMK. VU590 can

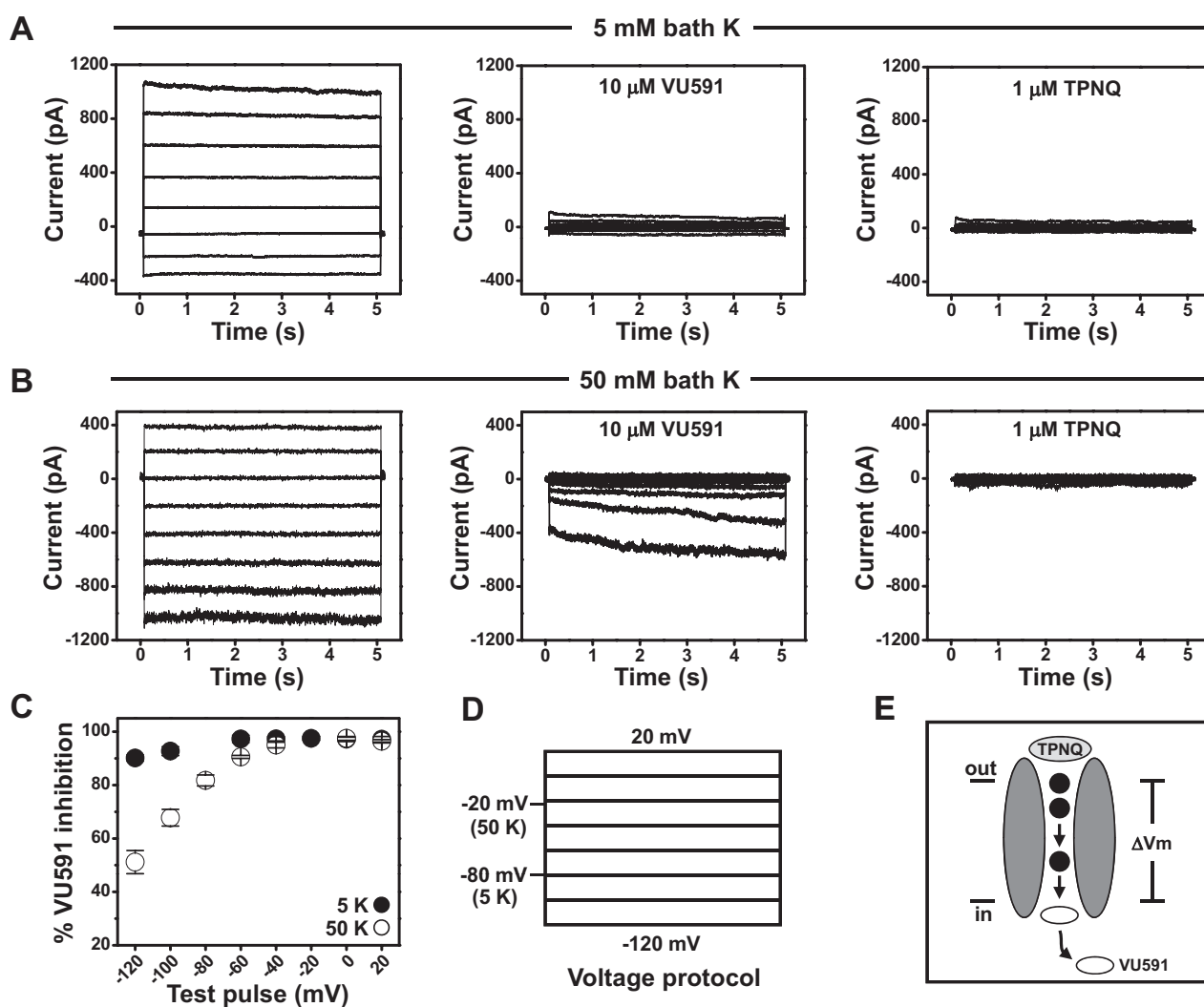


**Fig. 3.** VU591 is a ROMK channel pore blocker. **A**, representative whole-cell current responses to voltage steps from a holding potential of  $-80$  mV (see protocol in **D**) in a bath solution with  $[K^+]$  of 5 mM recorded in rat ROMK transiently transfected HEK-293 cells. Left, control conditions; middle, 10  $\mu$ M VU591; right, 1  $\mu$ M TPNQ. **B**, representative whole-cell current traces with voltage steps from a holding potential of  $-20$  mV (see protocol in **D**) in a bath solution with 50 mM  $K^+$  recorded in rat ROMK1 transiently transfected HEK-293 cells. Left, control conditions; middle, 10  $\mu$ M VU591; right, 1  $\mu$ M TPNQ. **C**, percentage VU591 inhibition was calculated at each voltage with 5 and 50 mM extracellular  $K^+$  after subtracting leak current defined as residual current with 1  $\mu$ M TPNQ. Inhibition at the holding potential ( $-80$  mV in 5 mM  $K^+$  and  $-20$  mV in 50 mM  $K^+$ ) was not determined given the low current amplitudes near  $E_K$ . **D**, voltage step protocol involving a holding potential near equilibrium potential for  $K^+$  ( $-80$  and  $-20$  mV in 5 and 50 mM extracellular  $K^+$ , respectively) with first step to 20 mV followed by lower steps in 20-mV increments with intervening periods of 200 ms at the holding potential. Step duration was extended to 5 s to reach near steady-state conditions, particularly in the presence of VU591. **E**, model for VU591 and TPNQ block of ROMK currents (see text for further details).

TABLE 2

Plasma protein binding of VU591

Percentage VU591, warfarin (control), and verapamil (control) bound to human or rat serum protein are shown. Data are mean  $\pm$  S.D. from 2 replicate experiments.

	Human	Rat
	<i>% bound</i>	
VU591	99.14 $\pm$ 0.0056	98.39 $\pm$ 0.0010
Warfarin	99.62 $\pm$ 0.0002	99.57 $\pm$ 0.0003
Verapamil	93.41 $\pm$ 0.0088	97.14 $\pm$ 0.0037

be displaced from its binding site by inwardly directed  $K^+$  ions, a phenomenon termed “knock-off,” suggesting that it blocks the intracellular pore of the channel (Lewis et al., 2009). If VU590 and VU591 interact with the same sites, we postulated that VU591 would also exhibit knock-off. To test this hypothesis, HEK-293 cells were bathed in solutions containing 5 or 50 mM  $K^+$  and 10  $\mu$ M VU591 to block ROMK (Fig. 3, A and B). The cells were subsequently voltage-clamped at a holding potential of  $-80$  mV (5  $K^+$ ) or  $-20$  mV (50  $K^+$ ) and then stepped for 5 s to test voltages between 20 and  $-120$  mV in 20-mV increments (Fig. 3D). The mean  $\pm$  S.E.M. percentage block at the end of each test pulse is shown in Fig. 3C. In 5 mM  $K^+$ , VU591 inhibition exhibited a trend toward reduced block with hyperpolarization but was not statistically significant ( $P = 0.081$ ). However, elevation of extracellular  $K^+$  caused a dramatic decrease in percentage block at hyperpolarizing potentials ( $P < 0.001$ ). To confirm that the hyperpolarization- and high  $K^+$ -induced current is not carried by endogenous inward rectifiers that are insensitive to VU591, we showed the current could be inhibited by the ROMK blocker tertiapin-Q (TPNQ; Fig. 3, A and B, right). Taken together, these data support the hypothesis that the VU591 binding site lies within the intracellular ion permeation pathway near the VU590 binding site.

**VU591 Serum Protein Binding and Metabolic Stability.** The utility of VU591 as a probe of ROMK function in whole-animal studies will depend in part on its propensity to bind serum protein and susceptibility to degradation by liver metabolic enzymes. We therefore measured the protein binding and metabolic stability of VU591 in vitro. Binding of VU591 to human and rat serum protein was compared with the anticoagulant warfarin, a highly protein-bound drug, and verapamil as controls. The results, which are summarized in Table 2, show that VU591 is almost entirely protein-bound in human serum but that approximately 2% of the inhibitor is free in rat serum.

The metabolic stability of VU591, verapamil, and propranolol in human and rat liver microsomes was assessed next. The results are summarized in Fig. 4. After a 15-min incu-

bation period, approximately 60 to 80% of VU591 remained intact in rat and human microsomes. In both species, VU591 was more stable than verapamil or propranolol.

## Discussion

Since Ho et al. (1993) and Zhou et al. (1994) cloned ROMK nearly 20 years ago, the small-molecule pharmacology of the Kir family has remained largely undeveloped and limited to barium, cesium, and a handful of nonselective drugs exhibiting weak off-target activity toward Kir channels (for review, see Bhave et al., 2010). The slow progress in the field has hindered efforts to understand the physiology, clinical relevance, and therapeutic potential of certain Kir channels. Part of our motivation for developing small-molecule inhibitors of ROMK is to test the long-standing hypothesis that ROMK is a target for a novel class of antihypertensive drug.

The discovery (Simon et al., 1996) that patients with antenatal Bartter syndrome (ABS) carry autosomal recessive loss-of-function mutations in the gene encoding ROMK (*KCNJ1*) seems to argue against ROMK as a viable therapeutic target. Patients with ABS frequently present with hypercalciuria, metabolic alkalosis, and hypokalemia in addition to low-to-normal blood pressure (Bartter et al., 1962; Peters et al., 2002). It is noteworthy, however, that Ji et al. (2008) identified heterozygous carriers of *KCNJ1* mutations with lower blood pressure but no reported symptoms of ABS. Likewise, Tobin et al. (2008) identified small nucleotide polymorphisms in *KCNJ1* that were associated with lower blood pressure in the general population. No associations with serum  $K^+$  were found (Tobin et al., 2008). Taken together, these studies suggest that a partial reduction in ROMK function may lower blood pressure without causing derangements in serum electrolytes.

It remains to be seen whether pharmacological inhibition of ROMK in genetically healthy persons will induce diuresis. The canonical 30-pS channel attributed to ROMK is coexpressed with a molecularly unidentified 70-pS channel in the TAL, where it is estimated to contribute up to 80% of apical  $K^+$  conductance (Wang and Lu, 1995). Like the 30-pS channel, the 70 pS channel is absent in *KCNJ1*( $-/-$ ) knockout mice, leading Lu et al. (2004) to propose that ROMK subunits form part of the 70-pS channel. It is conceivable that the volume disturbances caused by mutations in *KCNJ1* reflect loss of both conductances. It will be important to determine whether VU591 inhibits one or both conductances to facilitate the interpretation animal studies assessing VU591's diuretic properties. Given the selectivity of VU591 for ROMK over other inward rectifiers, we postulate that VU591 will

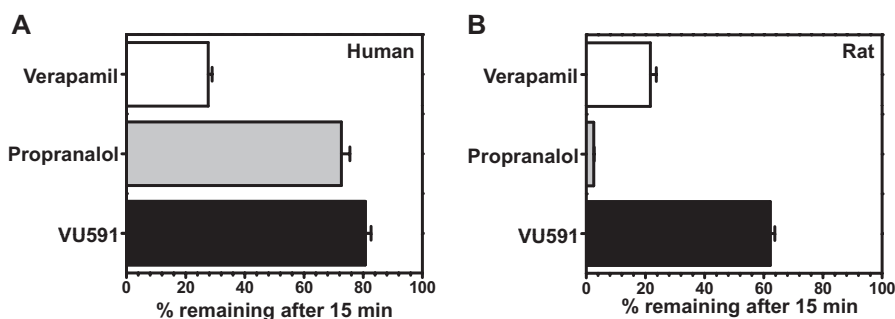


**Fig. 4.** Metabolic stability of VU591 in human or rat liver microsomes. Percentage VU591, verapamil (control), and propranolol (control) remaining after a 15-min incubation are shown. Data are means  $\pm$  S.D. from two replicate experiments.

not inhibit the 70-pS conductance if it is carried by a heteromeric channel. Testing this hypothesis should ultimately shed light on the molecular structure and physiology of the 70-pS channel.

As a first step toward determining whether VU591 is active on native ROMK channels expressed in the distal nephron, we measured net  $K^+$  ( $J_K$ ) and  $Na^+$  ( $J_{Na}$ ) transport in isolated-perfused rat CDs before and after luminal perfusion with 10  $\mu$ M VU591. Data summarized in Supplemental Fig. 6 show that VU591 significantly inhibited  $J_K$  from  $-7.0 \pm 1.3$  (control) to  $-3.6 \pm 0.6$  (VU591)  $\text{pmol} \cdot \text{min}^{-1} \cdot \text{mm}^{-1}$  ( $n = 4$ ;  $P < 0.05$ ) in CD perfused at  $1.5 \pm 0.4$  and  $1.2 \pm 0.1$  ( $P > 0.05$ )  $\text{nl} \cdot \text{min}^{-1} \cdot \text{mm}^{-1}$ , respectively. Luminal VU591 had no significant effect on  $J_{Na}$  in these same tubules ( $16.1 \pm 2.6$  and  $12.5 \pm 0.6$   $\text{pmol} \cdot \text{min}^{-1} \cdot \text{mm}^{-1}$ ;  $P > 0.05$ ). These preliminary data suggest strongly that VU591 inhibits native ROMK in rat kidney and that ROMK mediates, at least in part, basal  $K^+$  secretion in the collecting duct. VU591 used in combination with other blockers should help to elucidate the relative contribution of ROMK and other  $K^+$  channels (e.g., BK, Kv1.3) to renal  $K^+$  transport during various physiological and pathophysiological states.

VU591 inhibited hERG activity by approximately 25% (Ta-

ble 1). Our data may actually underestimate the degree of hERG block observed in mammals because many drugs exhibit decreased potencies toward hERG expressed in *X. laevis* oocytes (Witchel et al., 2002). If VU591 is indeed a potent hERG blocker in cardiac myocytes, this might limit the choice of animal models for in vivo studies to mice, in which hERG does not play a critical role in cardiac function (Wang et al., 1996).

We found that 10 to 30  $\mu$ M VU591 inhibited ROMK current at  $-120$  mV by approximately 90%, raising the possibility that VU591 is a partial antagonist of the channel. However, it should be noted VU591 inhibition increased to  $\sim 97\%$  at  $-60$  mV (Fig. 3C). We therefore propose that VU591 is a full antagonist exhibiting weak voltage-dependent unblock at strong negative potentials. This property should have minimal effects on its potency in cells with typical resting potentials above equilibrium potential for  $K^+$ .

Why does the addition of the ether oxygen to the aliphatic linker region of BNBI (Fig. 5B) increase its potency toward ROMK? We explored this question using the SurfexSim optimized flexible alignment algorithm (see *Materials and Methods*), which superimposes common chemical features of VU590, BNBI, and VU591, including hydrogen bond donors,

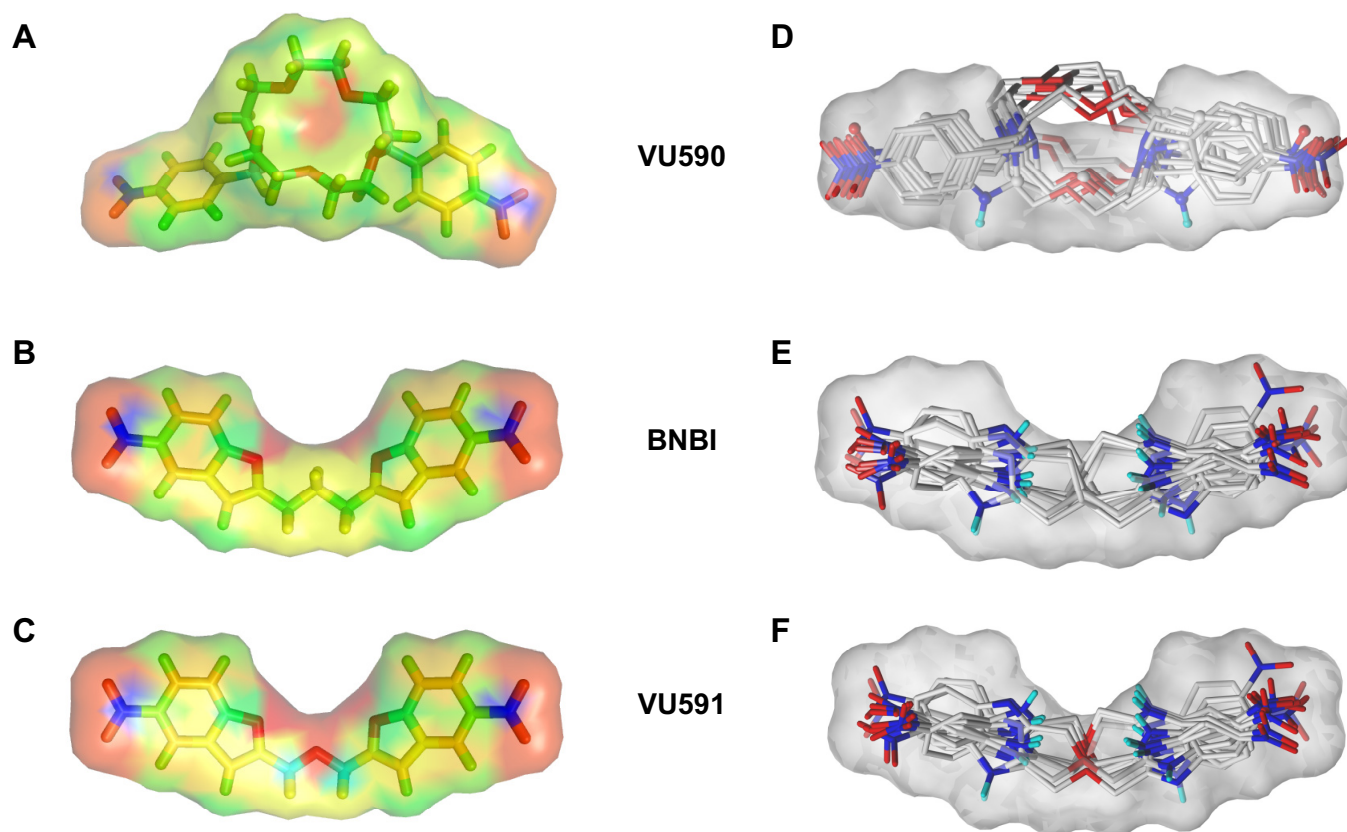


**Fig. 5.** Addition of negative surface electrostatic potential through an ether linkage increases ROMK inhibitor potency. Two primary screening hits, VU590 (A) and BNBI (B), share the common substructure of flanking nitrophenyl groups linked by alkyl chains of different length and composition. Visualization of the distribution of electrostatic properties was achieved by displaying atom-centered point charges from the Merck Molecular Mechanics Forcefield (MMFF94) on a Connolly surface of each molecule (A–C). Atomic charge values are indicated by color ramp ranges from negative (red) to positive electrostatic potential (blue). When VU590 is flexibly aligned with BNBI (see *Materials and Methods*) and displayed in a similar conformation, localization of negative electrostatic potential in the middle portion of the molecule is observed. This is consistent with the rationale used to generate increased potency in VU591 (C) and suggests that the negative electrostatic potential of the ether linker contributes to the increased potency of VU591 toward ROMK. Right, conformational ensembles generated by SurfexSim (SybylX 1.1; Tripos) from the 10 top-scoring aligned conformers of VU590 (D), BNBI (E), and VU591 (F). The surface of the best-scoring, most similar alignment (gray Connolly surface) highlights increased flexibility within and flanking the VU590 macrocyclic linker relative to the bicyclic rings and propyl/ether linker of BNBI/VU591 that is consistent with enhanced ROMK selectivity observed experimentally with VU591 versus VU590.

electron-rich imidazole nitrogen atoms, ether oxygen atoms, and nitrophenyl groups. The resulting structural alignments contained conformers that concentrate negative electrostatic potential by bringing together the ether oxygen and both electron-rich imidazole nitrogen atoms of VU591 (Fig. 5C) in close spatial proximity with the macrocycle ring nitrogens and an ether oxygen of VU590 (Fig. 5A). This supports the notion that the greater potency of VU591 is due to an increased electron donor potential (and hydrogen bond acceptor potential) of the ether linker that stabilizes ligand interactions with a polar portion of the ROMK pore.

The flexible and bulky VU590 macrocycle linker (Fig. 5D) could contribute to the compound's low-affinity block of Kir7.1 (Fig. 1C). Its absence in BNBI (Fig. 5E) and VU591 (Fig. 5F) may therefore contribute toward selectivity for ROMK. The SurflexSim alignment method also minimizes nonoverlapping compound volume and aligns chemical features as part of the conformational search process (see *Materials and Methods*). The number of VU590 conformational ensemble atoms lying outside of the Connolly surface of the optimized BNBI/VU591 alignment (Fig. 5D) clearly exceeds those of BNBI and VU591 (Fig. 5, E and F). The VU590 linker is bulkier and more flexible and therefore may access additional less selective and lower-affinity binding sites in Kir7.1 because of these properties. We postulate that the more rigid imidazole scaffold of BNBI and VU591 contributes to increased selectivity for ROMK inhibition because the demonstrably more flexible VU590 has additional activity at Kir7.1. These issues will be addressed in future studies to define the VU590 and VU591 structure-activity relationships and molecular binding sites in ROMK and Kir7.1.

#### Acknowledgments

We thank Sreedatta Banerjee and members of the Nanion team for expert technical assistance, Dr. Eric Delpire for providing oocytes, Aihua Bian (Vanderbilt University Department of Biostatistics) for assistance with multivariate statistical analysis, and members of the Kupersmidt laboratory for advice on hERG recordings.

#### Authorship Contributions

*Participated in research design:* Bhave, Chauder, Liu, Dawson, Kadakia, Lewis, Meiler, Weaver, Satlin, Lindsley, and Denton.

*Conducted experiments:* Bhave, Chauder, Liu, Dawson, Kadakia, Nguyen, and Lewis.

*Contributed new reagents or analytic tools:* Chauder, Dawson, and Meiler.

*Performed data analysis:* Bhave, Chauder, Liu, Dawson, Kadakia, Lewis, Satlin, Nguyen, and Denton.

*Wrote or contributed to the writing of the manuscript:* Chauder, Dawson, Satlin, and Denton.

#### References

Bartter FC, Pronove P, Gill JR Jr, and Maccardle RC (1962) Hyperplasia of the juxtaglomerular complex with hyperaldosteronism and hypokalemic alkalosis. A new syndrome. *Am J Med* **33**:811–828.

Bhave G, Lonergan D, Chauder BA, and Denton JS (2010) Small-molecule modulators of inward rectifier K channels: recent advances and future possibilities. *Future Med Chem* **2**:757–774.

Carrisoza-Gaytán R, Salvador C, Satlin LM, Liu W, Zavilowitz B, Bobadilla NA,

Trujillo J, and Escobar LI (2010) Potassium secretion by voltage-gated potassium channel Kv1.3 in the rat kidney. *Am J Physiol Renal Physiol* **299**:F255–F264.

Chuang H, Jan YN, and Jan LY (1997) Regulation of IRK3 inward rectifier K<sup>+</sup> channel by m1 acetylcholine receptor and intracellular magnesium. *Cell* **89**:1121–1132.

Clark MA, Humphrey SJ, Smith MP, and Ludens JH (1993) Unique natriuretic properties of the ATP-sensitive K<sup>+</sup>-channel blocker glyburide in conscious rats. *J Pharmacol Exp Ther* **265**:933–937.

Fallen K, Banerjee S, Sheehan J, Addison D, Lewis LM, Meiler J, and Denton JS (2009) The Kir channel immunoglobulin domain is essential for Kir1.1 (ROMK) thermodynamic stability, trafficking and gating. *Channels (Austin)* **3**:57–68.

Grimm PR and Sansom SC (2007) BK channels in the kidney. *Curr Opin Nephrol Hypertens* **16**:430–436.

Grobbee DE and Hoes AW (1995) Non-potassium-sparing diuretics and risk of sudden cardiac death. *J Hypertens* **13**:1539–1545.

Hebert SC, Desir G, Giebisch G, and Wang W (2005) Molecular diversity and regulation of renal potassium channels. *Physiol Rev* **85**:319–371.

Ho K, Nichols CG, Lederer WJ, Lytton J, Vassilev PM, Kanazirska MV, and Hebert SC (1993) Cloning and expression of an inwardly rectifying ATP-regulated potassium channel. *Nature* **362**:31–38.

Jain AN (2000) Morphological similarity: a 3D molecular similarity method correlated with protein-ligand recognition. *J Comput Aided Mol Des* **14**:199–213.

Ji W, Foo JN, O'Roak BJ, Zhao H, Larson MG, Simon DB, Newton-Cheh C, State MW, Levy D, and Lifton RP (2008) Rare independent mutations in renal salt handling genes contribute to blood pressure variation. *Nat Genet* **40**:592–599.

Jiang B, Sun X, Cao K, and Wang R (2002) Endogenous Kv channels in human embryonic kidney (HEK-293) cells. *Mol Cell Biochem* **238**:69–79.

Lewis LM, Bhave G, Chauder BA, Banerjee S, Lornsen KA, Redha R, Fallen K, Lindsley CW, Weaver CD, and Denton JS (2009) High-throughput screening reveals a small-molecule inhibitor of the renal outer medullary potassium channel and Kir7.1. *Mol Pharmacol* **76**:1094–1103.

Lu M, Wang T, Yan Q, Wang W, Giebisch G, and Hebert SC (2004) ROMK is required for expression of the 70-pS K channel in the thick ascending limb. *Am J Physiol Renal Physiol* **286**:F490–F495.

Macdonald JE and Struthers AD (2004) What is the optimal serum potassium level in cardiovascular patients? *J Am Coll Cardiol* **43**:155–161.

Milligan CJ, Li J, Sukumar P, Majeed Y, Dallas ML, English A, Emery P, Porter KE, Smith AM, McFadzean I, et al. (2009) Robotic multiwell planar patch-clamp for native and primary mammalian cells. *Nat Protoc* **4**:244–255.

Ookata K, Tojo A, Suzuki Y, Nakamura N, Kimura K, Wilcox CS, and Hirose S (2000) Localization of inward rectifier potassium channel Kir7.1 in the basolateral membrane of distal nephron and collecting duct. *J Am Soc Nephrol* **11**:1987–1994.

Peters M, Jeck N, Reinalter S, Leonhardt A, Tönshoff B, Klaus GG, Konrad M, and Seyberth HW (2002) Clinical presentation of genetically defined patients with hypokalemic salt-losing tubulopathies. *Am J Med* **112**:183–190.

Pluznick JL, Wei P, Carmines PK, and Sansom SC (2003) Renal fluid and electrolyte handling in BKCa-beta1<sup>-/-</sup> mice. *Am J Physiol Renal Physiol* **284**:F1274–F1279.

Rieg T, Vallon V, Sausbier M, Sausbier U, Kaissling B, Ruth P, and Osswald H (2007) The role of the BK channel in potassium homeostasis and flow-induced renal potassium excretion. *Kidney Int* **72**:566–573.

Simon DB, Karet FE, Rodriguez-Soriano J, Hamdan JH, DiPietro A, Trachtman H, Sanjad SA, and Lifton RP (1996) Genetic heterogeneity of Bartter's syndrome revealed by mutations in the K<sup>+</sup> channel, ROMK. *Nat Genet* **14**:152–156.

Tobin MD, Tomaszewski M, Braund PS, Hajat C, Raleigh SM, Palmer TM, Caulfield M, Burton PR, and Samani NJ (2008) Common variants in genes underlying monogenic hypertension and hypotension and blood pressure in the general population. *Hypertension* **51**:1658–1664.

Wang L, Feng ZP, Kondo CS, Sheldon RS, and Duff HJ (1996) Developmental changes in the delayed rectifier K<sup>+</sup> channels in mouse heart. *Circ Res* **79**:79–85.

Wang T, Wang WH, Klein-Robbenhaar G, and Giebisch G (1995a) Effects of a novel K<sub>ATP</sub> channel blocker on renal tubule function and K channel activity. *J Pharmacol Exp Ther* **273**:1382–1389.

Wang T, Wang WH, Klein-Robbenhaar G, and Giebisch G (1995b) Effects of glyburide on renal tubule transport and potassium-channel activity. *Ren Physiol Biochem* **18**:169–182.

Wang W and Lu M (1995) Effect of arachidonic acid on activity of the apical K<sup>+</sup> channel in the thick ascending limb of the rat kidney. *J Gen Physiol* **106**:727–743.

Welling PA and Ho K (2009) A comprehensive guide to the ROMK potassium channel: form and function in health and disease. *Am J Physiol Renal Physiol* **297**:F849–F863.

Witchel HJ, Milnes JT, Mitcheson JS, and Hancox JC (2002) Troubleshotting problems with in vitro screening of drugs for QT interval prolongation using HERG K<sup>+</sup> channels expressed in mammalian cell lines and *Xenopus* oocytes. *J Pharmacol Toxicol Methods* **48**:65–80.

Yu SP and Kerchner GA (1998) Endogenous voltage-gated potassium channels in human embryonic kidney (HEK293) cells. *J Neurosci Res* **52**:612–617.

Zhou H, Tate SS, and Palmer LG (1994) Primary structure and functional properties of an epithelial K channel. *Am J Physiol* **266**:C809–C824.

**Address correspondence to:** Dr. Jerod S. Denton, T4208 Medical Center North, 1161 21st Avenue South, Nashville, TN 37232. E-mail: jerod.s.denton@vanderbilt.edu